SCIENTIFIC REPORTS

OPEN

SUBJECT AREAS:
PLASMA PHYSICS
CONDENSED-MATTER PHYSICS

Received
6 May 2014

Accepted
15 July 2014

Published
31 July 2014

Correspondence and requests for materials should be addressed to P.Z. (zhang_ping@iapcm.ac.cn) or J.Y. (yan_jun@iapcm.ac.cn)

# Quantum molecular dynamics study of expanded beryllium: Evolution from warm dense matter to atomic fluid

Dafang Li[1], Haitao Liu[1], Siliang Zeng[1], Cong Wang[1,2], Zeqing Wu[1], Ping Zhang[1,2] & Jun Yan[1,2]

[1]Institute of Applied Physics and Computational Mathematics, P.O. Box 8009, Beijing 100088, People's Republic of China, [2]Center for Applied Physics and Technology, Peking University, Beijing 100871, People's Republic of China.

**By performing quantum molecular dynamics (QMD) simulations, we investigate the equation of states, electrical and optical properties of the expanded beryllium at densities two to one-hundred lower than the normal solid density, and temperatures ranging from 5000 to 30000 K. With decreasing the density of Be, the optical response evolves from the one characteristic of a simple metal to the one of an atomic fluid. By fitting the optical conductivity spectra with the Drude-Smith model, it is found that the conducting electrons become localized at lower densities. In addition, the negative derivative of the electrical resistivity on temperature at density about eight lower than the normal solid density demonstrates that the metal to nonmetal transition takes place in the expanded Be. To interpret this transition, the electronic density of states is analyzed systematically. Furthermore, a direct comparison of the Rosseland opacity obtained by using QMD and the standard opacity code demonstrates that QMD provides a powerful tool to validate plasma models used in atomic physics approaches in the warm dense matter regime.**

Expanded liquid metals are focused in a series of important research areas because they evolve through various phases with associate transitions in the electrical and thermodynamic properties[1]. In this thermodynamic regime, often labeled as warm dense matter (WDM), matter is partially dissociated, ionized and degenerate, which makes the description of the dynamical, electrical and optical properties extremely difficult. Experimental studies on electrical and thermodynamic properties of the metals with low critical temperatures such as mercury (Hg), rubidium (Rb) and cesium (Cs) have been widely made and the aspect of metal-nonmetal transition has been clarified[2–4]. The models to describe the metal-nonmetal transitions in very different physical systems from ordered solids to disordered fluids and plasmas and the important physical effects therein have already been discussed in detail by Mott, Hubbard, Anderson, Edwards *et al.* and Redmer *et al.*[5–11]. It has been pointed out that the transitions of these very diverse systems are driven by the complex many-body nature of the respective interactions similarly[11]. In the case of metals with higher critical points, the first experimental data were obtained on aluminum with the dynamic methods recently[12]. Then, the metal-nonmetal transitions in expanded nickel[13], titanium[14], iron[15], and tungsten[16] were studied. One of the motivations of these studies was to find out the interrelation between the liquid-vapor and the metal-nonmetal transitions. However, to our knowledge, no data on expanded beryllium (Be), another refractory metal with high critical point, have been reported. As known, beryllium at warm dense regime is of particular importance because of its technological applications. Specifically, it is a potential ablator material in inertial confinement fusion (ICF) capsules and is also relevant for astrophysics. The optical and thermodynamic properties of Be decide the compressibility of the capsule, laser absorption, and instability growth at the fuel-ablator interface in ICF[17].

The experimental and theoretical studies of warm dense Be mainly focused on its compressed state. Using the shock waves generated by underground nuclear explosives, Ragan[18] and Nellis *et al.*[19] obtained the hugoniot of Be up to about 18 Mbar. The high-intensity laser in laboratory can even probe similar pressure range[20]. Recently, the dynamic structure factor in uncompressed and threefold compressed Be were calculated using the *ab initio* approach[21]. Wang *et al.* reported the equation of state (EOS) and transport properties of Be for densities from 4.0 to 6.0 g/cm$^3$ and temperatures from 1.0 to 10.0 eV based on the quantum molecular dynamics (QMD) simulations[22]. However, the properties of thermal-expanded Be are still yet to be investigated. In the process of thermal expansion, a series of related questions show up: how the structure of Be evolves, whether the metal-nonmetal transition takes place, if yes, and then how does this transition affect its thermodynamic and optical properties. The answers to these questions would provide a good understanding of the structural, electronic and

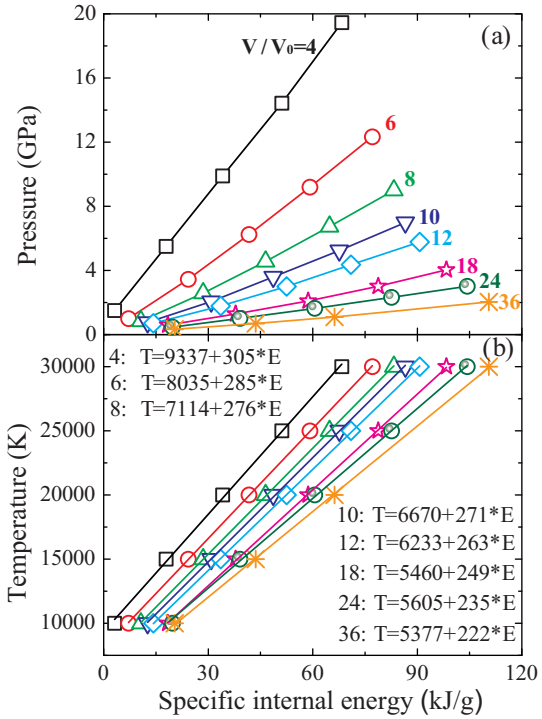


**Figure 1** | (a) Pressure and (b) temperature versus specific internal energy along eight selected isochores ($V/V_0 = 4$ (square), 6 (circle), 8 (uptriangle), 10 (downtriangle), 12 (diamond), 18 (star), 24 (sphere) and 36 (cross)). The lines are linear fits of the simulated results along the isochores correspondingly.

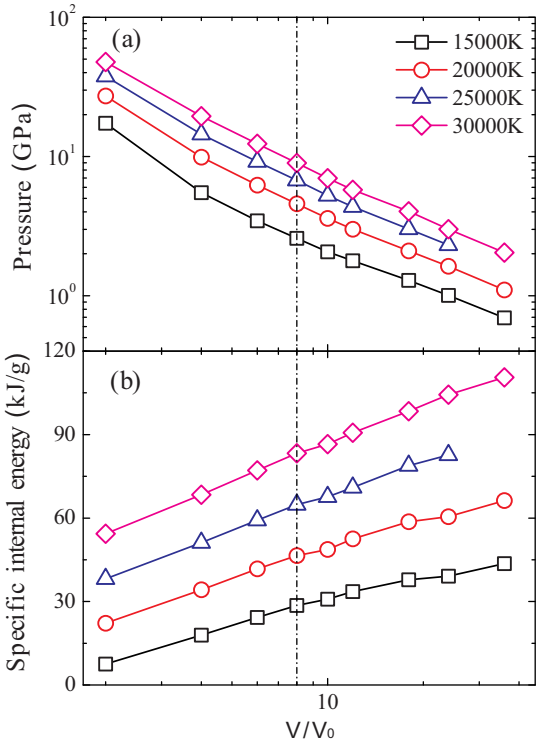


**Figure 2** | (a) Pressure and (b) specific internal energy versus the relative volume value along four selected isotherms.

dynamic properties of warm dense Be and the basic mechanisms that are responsible for these properties. From the theoretical point of view, QMD[23,24] is particularly suited for this kind of problems because no assumptions on the species involved or in the ionization state are needed. In particular, when combined with the Kubo-Greenwood formulation, QMD method can produce a consistent set of structural, electrical and optical properties from the same simulation. QMD has been successfully used on several expanded metals and predicted their metal-nonmetal transitions precisely[12–14,25–32].

In this paper, we introduce QMD method, where the active electrons are treated in a full quantum mechanical way within the finite temperature density functional theory (FTDFT), to study the expanded Be. We calculate its EOS, electrical and optical properties to explore the evolution of Be as density and temperature change. The EOS are extracted from a series of QMD simulations of Be at densities of two to one-hundred lower than the normal solid density and temperature ranging from 5000 K to 30000 K. Using the configuration trajectories, the optical spectra are obtained from Kubo-Greenwood formula, from which the DC conductivity are determined. We analyze the variation of electronic density of states with respect to density and temperature to interpret the physics of the metal-nonmetal transition in expanded Be. The paper is organized as follows. In Sec. II, we briefly describe the simulation details and computational method in determining the optical conductivity. The results of EOS, electrical and optical properties are discussed in Sec. III. Finally, we close our paper with a summary of our main results.

## Results

**Equation of State.** The EOS data for expanded Be are derived from the QMD simulations, which could describe various transient processes such as dissociation or association of chemical bonds and ionization or recombination induced by temperature or density without any approximation. The internal energy equals to the sum of the ion kinetic energy and the time average of DFT potential energy. The pressure consists of the contributions from the electronic and ionic components, which come from, respectively, the derivative of the total energy with respect to the Kohn-Sham electronic orbitals and the ideal gas expression since the ions move classically. In Fig. 1 the variations of pressure and temperature as a function of specific internal energy along eight selected isochores are shown. These relative volume values are $V/V_0 = 4$, 6, 8, 10, 12, 18, 24, and 36, respectively, in which the normal solid volume $V_0 = 4.87$ cm$^3$/mol. We can see from Fig. 1(a) that the EOS shows a systematic behavior for each isochore that the pressure and temperature increase almost linearly with the specific internal energy, similar as in expanded aluminum[12]. The relations between temperature (in unit of K) and specific internal energy (in unit of kJ/g) are found to have the following forms of $T = 9337 + 305E$ for $V/V_0 = 4$, $T = 8035 + 285E$ for $V/V_0 = 6$, $T = 7114 + 276E$ for $V/V_0 = 8$, $T = 6670 + 271E$ for $V/V_0 = 10$, $T = 6233 + 263E$ for $V/V_0 = 12$, $T = 5460 + 249E$ for $V/V_0 = 18$, $T = 5605 + 235E$ for $V/V_0 = 24$, and $T = 5377 + 222E$ for $V/V_0 = 36$. Since the experiment measured all quantities versus the internal energy variation while not temperature at present, it does not allow convenient comparisons with the other models. For expanded Be, the above relations map internal energies into temperatures, and could be used in future experimental study. In addition, we express the pressure (in unit of GPa) as a function of density $\rho$ (in unit of g/cm$^3$) and temperature $T$ as $P = 4.83 - 39.51454\rho + 0.00326\rho T$ through fitting all of these EOS data. It is indicated that the pressure is more dependent on density than temperature. Such a function should be applicable in hydrodynamic simulations for expanded Be conveniently.

The density effects on the EOS are highlighted in Fig. 2, which presents the pressure and internal energy versus the relative volume value for four selected isotherms with $T = 15000$, 20000, 25000, and 30000 K. As expected, the pressure decreases while specific internal energy increases with the relative volume systematically. In particu-

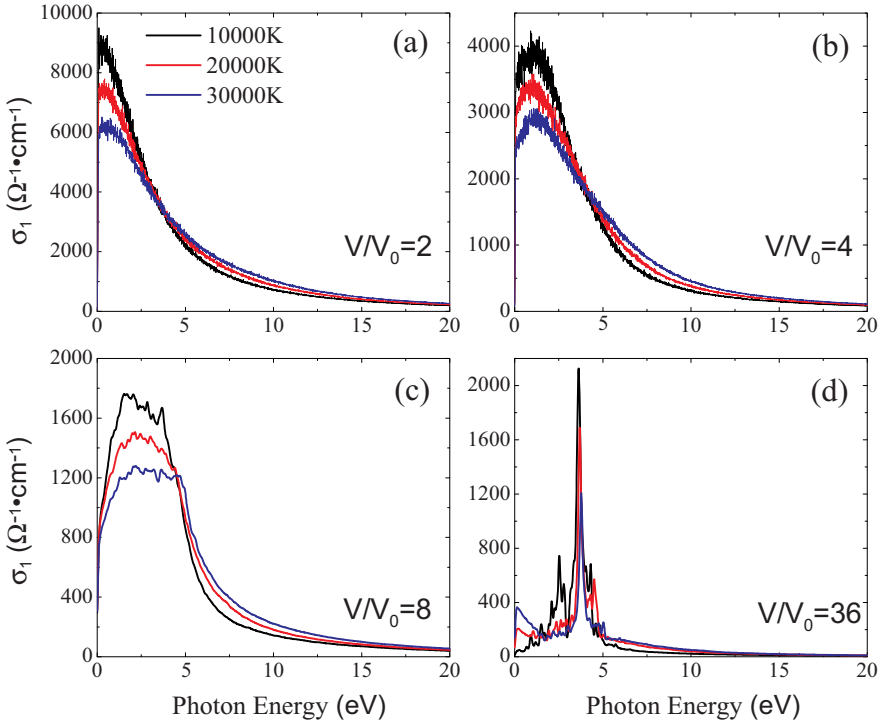


**Figure 3 | The real part of frequency-dependent electrical conductivity for the four selected relative volumes of (a) $V/V_0 = 2$; (b) $V/V_0 = 4$; (c) $V/V_0 = 8$; and (d) $V/V_0 = 36$ at temperatures of 10000 K (black), 20000 K (red) and 30000 K (blue).** Data have been averaged over 10 to 15 uncorrelated QMD configurations.

lar, it is noted that the internal energy keeps an almost linear relation with the relative volume until Be is expanded beyond eight times the normal solid volume. This means that the couplings between ions begin to become unimportant, indicating the appearance of an atomic phase.

**Electrical properties.** In general, thermal-expansion of a metal could lead to metal-nonmetal transition. We examine the variation of electrical conductivity of Be over the extensive density-temperature ranges to clarify the metal-nonmetal transition. Using the Kubo-Greenwood formula, we calculate the real part of frequency-dependent electrical conductivity for points with relative volume ranging from 2 to 100 and temperature from 5000 to 30000 K. The real part of electrical conductivities $\sigma_1(\omega)$ for four selected relative volumes of $V/V_0 = 2$, 4, 8, and 36 along the isotherms of 10000, 20000, and 30000 K are presented in Fig. 3. It is obvious that these four sets of plots at different relative volumes exhibit different characteristics. In Fig. 3(a), the optical conductivity is in good agreement with a Drude form ($\sigma_D(\omega) = \frac{n^* e^2 \tau/m}{1+\omega^2\tau^2}$, with $n^*$ and $\tau$ respectively representing the conducting electron number density and relaxation time) with the maximum located at zero frequency, which indicates the nearly free-electron nature of the system. Such a behavior has also been reported for solid and three-compressed Be at high temperatures in Ref. 21. As expected, the dc conductivities become larger with increasing the density and temperature when comparing with our results, which predicts better conducting behavior. As the system is expanded to four times $V_0$, the optical conductivity loses the Drude character with the main peak shifted to about 1 eV, as displayed in Fig. 3(b). To describe this case more appropriately, the Drude-Smith model[33] has been proposed in the following form

$$\sigma_{DS}(\omega) = \frac{n^* e^2 \tau/m}{1+\omega^2\tau^2}\left[1 + \frac{c(1-\omega^2\tau^2)}{(1+\omega^2\tau^2)}\right], \quad (1)$$

which is a generalization of the classical Drude model through including the memory effects of the successive collisions. In the formula, $c$ is a parameter of the memory effect. It equals to zero for the classical Drude model and falls into the range of 0 to $-1$ when the main peak is shifted to higher frequency. The vanishing of dc conductivity could lead to the value of $c = -1$. With the relative volume increased to eight, the main peak continues to shift even to the energies larger than $k_B T$, which corresponds to the case where the dc conductivity increases with temperature, opposite to the other two cases at lower relative volumes. It means that a metal-nonmetal transition takes place as Be is expanded to the volume larger than eight times $V_0$, which will be further discussed below. In addition, a small peak located between 3 $\sim$ 4 eV seems to shows up, which becomes more evident at larger volumes. At the volume of thirty-six times $V_0$, an atomic transition line from 2$s$ to 2$p$ arises, with the location depending on the temperature. For example, the peak is at 3.63 eV for $T$ = 10000 K and 3.78 eV for $T$ = 30000 K, in accordance with the atomic data. The shift comes from the increased ionization fraction of Be as the temperature is increased from 10000 K to 30000 K. It is confirmed that the expanded Be has evolved into an atomic phase from a condensed state.

By fitting the optical conductivity spectra with the more general Drude-Smith model in the functional form of $\sigma_1(\omega) = \frac{\sigma_{dc}}{(1+c)(1+\omega^2\tau^2)}\left[1 + \frac{c(1-\omega^2\tau^2)}{(1+\omega^2\tau^2)}\right]$, we get the dc conductivity $\sigma_{dc}$, relaxation time $\tau$, and the parameter $c$. Meanwhile, the conducting electron density $n^*$ and effective ionization fraction $\bar{Z}$ can be estimated as $n^* = \frac{m_e \sigma_{dc}}{e^2\tau}$ and $\bar{Z} = \frac{n^*\Omega}{N_i}$, respectively, with $\Omega$ being the volume of simulation cell and $N_i$ the number of ions in the cell. At the volume of two times of $V_0$, the fitting yields $\bar{Z}$ of about two and relaxation time of $1.57 \times 10^{-16}$ s for a temperature of 30000 K, in good agreement with an average ionization of 2.0 using both average atoms model[34] and COMPTRAO4 program within the partially ionized plasma model[35]. This average ionization fraction leads

to a coupling parameter $\Gamma = 14$ and a degeneracy parameter of $\theta = 0.12$, characteristic of a strong coupling and high degenerate plasma. At the largest volume of 100 times $V_0$ and temperature of 20000 K, an analysis of the optical conductivity gives an ionization fraction of 0.2, relaxation time of 5.37 fs and $c = -0.725$. The average atoms model[34] gives an ionization fraction of 0.21, while COMPTRA04 program[35] overestimates this value to be about 0.62. At such conditions, the system evolves into a weak coupled and low degenerated plasma with the corresponding coupling parameter and degeneracy parameter of 0.058 and 11.8, respectively.

The Drude-Smith fitted conductivities are presented in Fig. 4. It illustrates two competing behaviors: a strong lowering of the electrical conductivity with decreasing density which may induce metal-nonmetal transition and a thermal activation of the conductivity due to ionization. The dc conductivity of Be along three isotherms of 10000 K, 20000 K and 30000 K decreases with the density systematically with a power-law behavior, and reaches a nearly constant value at the lowest density explored. Furthermore, we note that for volumes larger than eight times $V_0$, the enhancement of the dc conductivity with the temperature is clearly evident. Such a behavior could be seen clearer in Fig. 5. At the low relative volume values, the resistivity increases with the temperature, which is a characteristic of a metal. The sign of the temperature dependence of the resistivity becomes negative as Be is expanded to eight times $V_0$, demonstrating the behavior of a semiconductor. Such a metal-nonmetal transition could also be confirmed from the point of the minimum metallic conductivity of about 2000 $\Omega^{-1}\text{cm}^{-1}$ for disordered systems[36], because we can see that the dc conductivity of Be is smaller than this value before the crossing points of these three plots.

A typical way to characterize the nonmetal-metal transition in expanded Be is the variation of electronic density of states (EDOS). In Fig. 6 we give the averaged EDOS at 10000 K for four different densities with a broadening of 0.03 eV. It can be seen that at $V/V_0 = 2$, EDOS clearly exhibits a free-electron-like behavior. As the volume increases, the EDOS is depressed in the vicinity of the Fermi level. At the largest volume of thirty-six times $V_0$ presented in Fig. 6(d), the EDOS shows a local atomic behavior and a gap opens.

**Optical properties.** The evolution of the media with lowering the density becomes clearer by examining the variation of the optical absorption coefficient along the 10000 K isotherm, as shown in Fig. 7. It is observed that the absorption coefficient increases rapidly in the photon energy range of a few eV, which mainly comes from the free-free contribution (also called inverse bremsstrahlung). As the volume is expanded, the most prominent change in the absorption coefficient is the shape and location of its main peak. At the lowest volume, the absorption coefficient shows the characteristic of a simple metal as described by the Drude model, with the maximum corresponding to a collective behavior associated with the transitions to the lowest excited states. With the volume further expanded up to twelve times $V_0$, more local features arise, especially the atomic transition line. At the volume of 100 times $V_0$, the peak become sharper due to the decrease of the ionization fraction of Be. Its location at about 3.63 eV corresponding to the position of 2*s* to 2*p* atomic transition. In addition, a valley around 2.0 eV is associated with the opening of the band gap as discussed above.

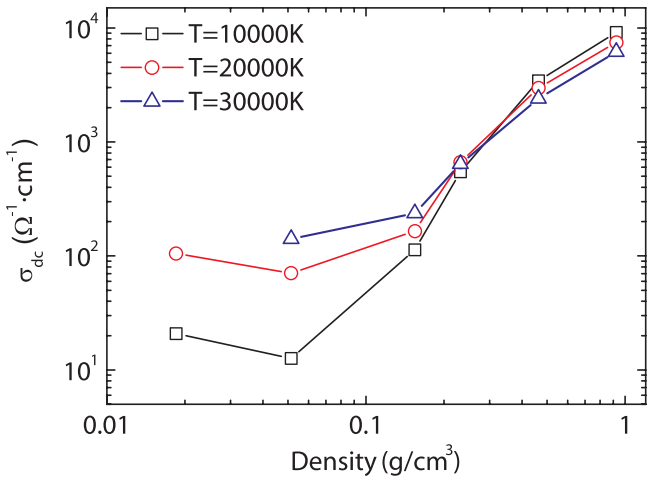


**Figure 4 | The variation of the dc conductivity of Be as a function of density for three isotherms.**

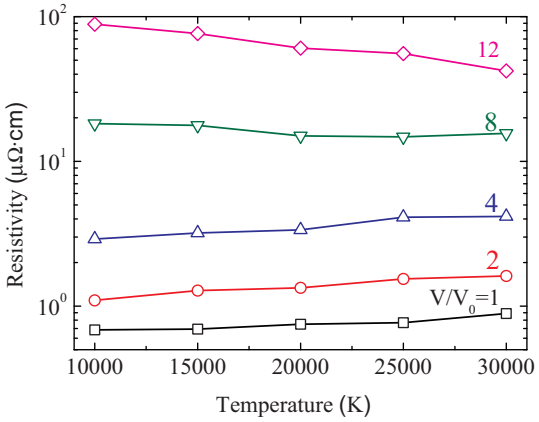


**Figure 5 | The resistivity variation with respect to the temperature along the five selected isochores of $V/V_0 = 1$ (square), $V/V_0 = 2$ (circle), $V/V_0 = 4$ (uptriangle), $V/V_0 = 8$ (downtriangle), and $V/V_0 = 12$ (diamond).**

In Fig. 8, we inspect the variation of the index of refraction with photon energy for different densities. For lower volumes than eight time $V_0$, the index of refraction decreases smoothly down to a minimum at an energy corresponding to the plasma frequency. As the volume increased to twelve time $V_0$, a mild maximum at a photon energy about 3.58 eV arises, followed by a marked minimum shifted to lower energy compared to that for lower volume. This suggests that atomic phase begins to appear under such density-temperature conditions. With the volume further expanded, the index of refraction first decreases to a minimum corresponding to a plasma frequency and then exhibits resonant profile at the position of atomic transition line, which is featured uniquely by the noninteracting atoms or ions. In fact, the plasma frequency could also be evaluated using the formula $\omega_p^2 = \frac{4\pi n^* e^2}{m_e}$ with the known ionization fraction. For example, at the lowest volume of two times $V_0$, the plasma frequency is calculated to be 13.06 eV corresponding to an ionization fraction $\bar{Z} = 2$, while for the highest volume of 100 times $V_0$, the plasma frequency is obtained as 0.21 with an ionization fraction of 0.027, in agreement with the behavior of the index of refraction shown in Fig. 8. Therefore, QMD is proved useful to describe the variation of the optical properties for a wide range of conditions from isolated atomic to the warm dense matter regime.

## Discussion

To understand the variations of the properties of expanded Be, we inspect the differences in the Rosseland mean opacities obtained using QMD and the standard opacity code LEDCOP[37]. The Rosseland mean opacity is calculated using Eq. (2) and based on QMD simulations for different density-temperature conditions. Figure 9 displays the variation of the Rosseland mean opacity for Be as obtained for a fixed temperature (10000 K) with increasing density (left panel) and fixed densities ($V/V_0 = 4$ and $V/V_0 = 12$) but increasing temperature (right panel). Comparisons with the data from LEDCOP are also included. Different from the QMD method

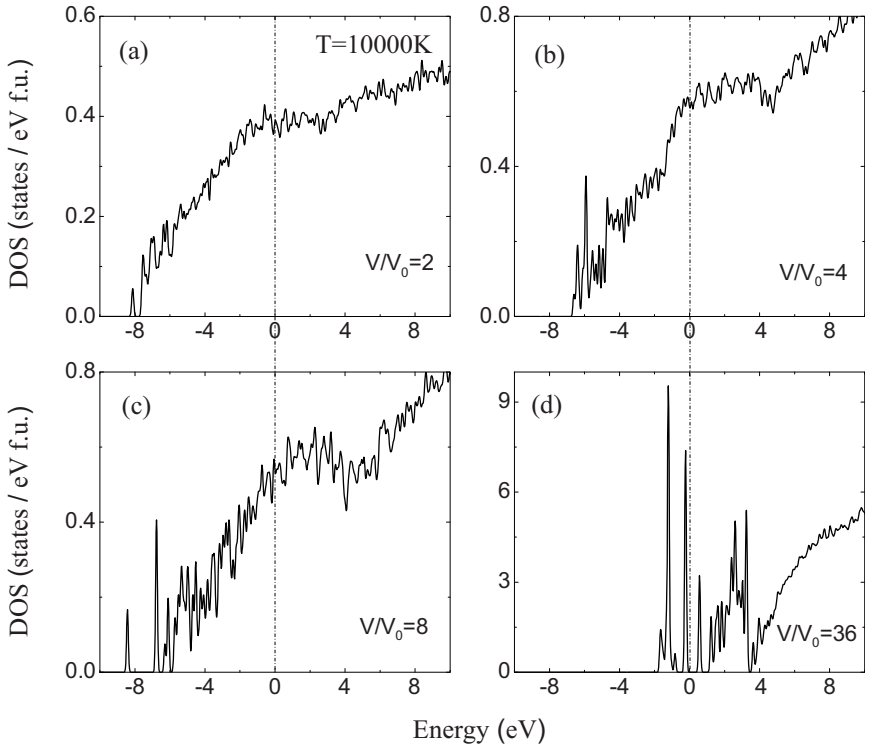


**Figure 6 | Electronic density of states of expanded Be at 10000 K for four densities.** Data have been averaged over 10 to 15 uncorrelated configurations. The zero of the energy scale shows the position of the Fermi level.

which gives a global optical spectra, LEDCOP opacity code calculates the contributions from atomic photoionization (bound-free), inverse bremsstrahlung (free-free), scattering and bound-bound transition separately. As seen in Fig. 9(a), for low densities, LEDCOP and the QMD show good agreement for Rosseland mean opacity. However, as the density increases, the LEDCOP and the QMD calculations depart, which results from the fact that various density effects, such as pressure ionization, are only introduced in a phenomenological fashion in LEDCOP. In addition, it is noted that the trend of the variation of QMD Rosseland mean opacity with expanding the volume changes beyond eight times $V_0$, which just coincides with the expansion induced metal-nonmetal transition. In Fig. 9(b), the Rosseland mean opacity decreases with temperature for these two densities, because at temperature of a few eV the opacity mainly comes from the free-free contribution.

In summary, we have systematically investigated the equation of state, electrical and optical properties of expanded Be at densities two to one-hundred lower than the normal solid density and temperatures ranging from 5000 to 30000 K through performing QMD simulations. The optical spectra demonstrate that as the density decreases, the system evolves from a simple metal to an atomic fluid. Through analyzing the variation of electrical conductivity, it is found that metal-nonmetal transition takes place in expanded Be at density about eight lower than the normal solid density, with the conducting electrons becoming localized. Furthermore, it is proved that QMD provides a powerful tool to describe from warm dense matter to atomic fluid.

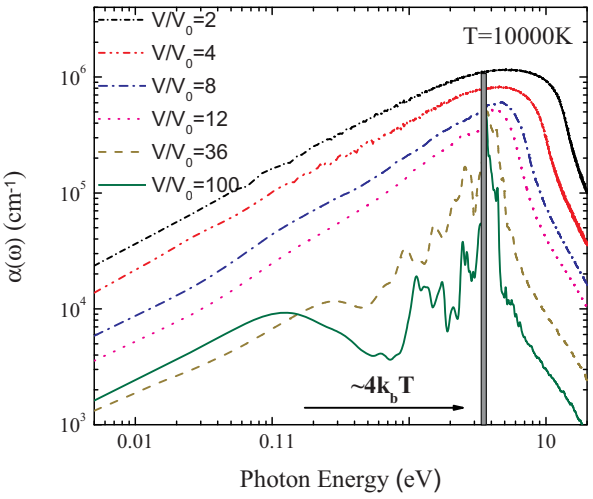


**Figure 7 | Absorption coefficient $\alpha(\omega)$ as a function of photon energy at $T = 10000$ K for different densities.** Bar at $4k_BT$ represents maximum region of contribution to the Rosseland mean opacity.

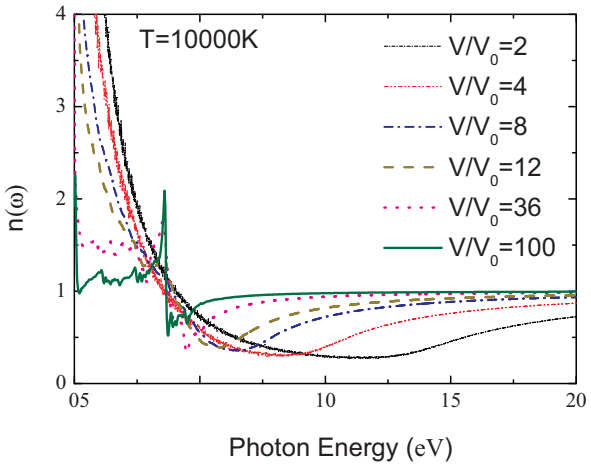


**Figure 8 | The index of refraction $n(\omega)$ as a function of photon energy at $T = 10000$ K for different densities.**

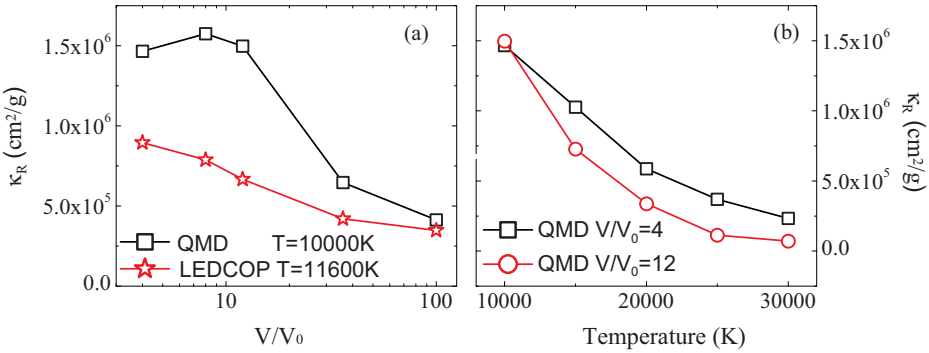


**Figure 9 | Variation of QMD and LEDCOP Rosseland mean opacities as a function of relative volume for a fixed temperature (left panel), and as a function of temperature for two fixed densities (right panel).**

## Methods

In the present application, ionic structures are first generated with the QMD package VASP (Vienna *ab initio* simulation package) developed at the Technical University of Vienna[38,39], in the framework of FT-DFT[23,40]. The interactions between ions and valence electrons are described using the all-electron projector augmented wave (PAW) potentials[41,42]. The exchange-correlation energy is treated on the level of generalized gradient approximation (GGA) using the Perdew-Wang 91 parametrization[43]. The electronic states are populated through a Fermi-Dirac distribution, with electronic temperature set equal to that of ions. Ions move classically according to the forces, which originate from the electron density and the ion-ion repulsion.

All of our QMD simulations employ the canonical (NVT) ensemble with Nosé-Hoover thermostat[44]. We select the densities ranging from two to one-hundred lower than the normal solid density ($V/V_0 = 2 \sim 100$) and temperatures from 5000 to 30000 K which cover a broad phases. Simulations are done at Γ point with 54 atoms for the densities from two to eighteen lower than the normal solid density and 8 atoms for the densities from twenty-four to one-hundred lower than the normal solid density in a cubic cell of the size appropriate to the considered density. More atoms are tested but the difference could be negligible. The plane-wave cutoff is fixed at 500.0 eV, which is tested to give good convergence for both total energy and pressure. For electronic properties calculations, $4 \times 4 \times 4$ Monkhorst-Pack[45] scheme $k$ points are used to sample the Brillouin zone. Integration of the equations of motion proceed with time step of $0.5 \sim 1.0$ fs for different pressure-temperature ranges. After about 3 ps the system is equilibrated and the subsequent 5 ps are taken to calculate the EOS and electronic properties as running averages. The ion temperature $T_i$ is fixed using Nosé-Hoover thermostat[44]. Additional convergence tests with respect to particle number and k-point Brillouin sampling are performed for several pressure-temperature conditions. In all cases, the internal energy is converged to less than 0.01 eV/atom and the pressure within an error bar of 2%.

Based on QMD simulated trajectories, $10 \sim 15$ configurations spaced by at least the correlation time are selected. For each of these configurations, the optical conductivities are obtained with the Kubo-Greenwood formulation[46,47] (atomic units),

$$\sigma_1(\omega) = \frac{2\pi}{3\omega\Omega}\sum_{\mathbf{k}} w(\mathbf{k}) \sum_{j=1}^{N}\sum_{i=1}^{N}\sum_{\alpha=1}^{3} \left[f(\epsilon_i,\mathbf{k}) - f(\epsilon_j,\mathbf{k})\right] \times \left|\langle\Psi_{j,\mathbf{k}}|\nabla_\alpha|\Psi_{i,\mathbf{k}}\rangle\right|^2 \delta(\epsilon_{j,\mathbf{k}} - \epsilon_{i,\mathbf{k}} - \hbar\omega), \quad (2)$$

where $\omega$ is the frequency, $\Omega$ the atomic volume, and $N$ the total number of bands used. $\Psi_{i,\mathbf{k}}$ and $\epsilon_{i,\mathbf{k}}$ are the electronic eigenstates and eigenvalues for the electronic state $i$ at a given $k$ point with the $w$ (**k**) **k**—point weighting factor, $f(\epsilon_{i,\mathbf{k}})$ stands for the Fermi distribution function. Other optical coefficients can be directly derived from the optical conductivity. In addition, the static limit $\omega \to 0$ of optical conductivity gives the dc conductivity $\sigma_{dc}$. As a particular application, the Rosseland mean opacity[48] is commonly used to represent the radiative property, which is expressed as

$$\frac{1}{\kappa_R(\rho,T)} = \frac{\int_0^\infty d\omega n^2(\omega)B'(\omega,T)\alpha(\omega)^{-1}}{\int_0^\infty d\omega n^2(\omega)B(\omega,T)}, \quad (3)$$

where $n$ ($\omega$) and $\alpha$ ($\omega$) are the frequency-dependent index of refraction and absorption coefficient, respectively. $B'$ ($\omega$, $T$) represents the derivative of the normalized Planck distribution with respect to temperature at a given $T$, a slowly varying function which peaks around $4k_BT$.


1. Landau, L. D. & Zeldovich, Ya. B. On the relation between the liquid and the gaseous states of metals. *Acta Physicochim. USSR* **18**, 194 (1943).
2. Kikoin, I. K. & Senchenkov, A. P. Electrical Conduction and the Equation of State of Mercury in the Temperature Range 0–2000°C and Pressure Region 200–5000 Atmospheres. *Fiz. Met. Metalloved.* **24**, 843–858 (1967).
3. Franz, G., Freyland, W. & Hensel, F. Thermodynamic and electric transport properties of fluid cesium and rubidium in M-NM transition region. *J. Phys. Colloques* **41**, C8–70 (1980).
4. Hensel, F. & Warren, W. W. *Fluid metals: the liquid-vapor transition of metals.* (Princeton, 1999).
5. Mott, N. F. The basis of the electron theory of metals, with special reference to the transition metals. *Proc. Phys. Soc. A* **62**, 416 (1949).
6. Hubbard, J. Electron correlations in narrow energy bands. III. An improved solution. *Proc. R. Soc. Lond. A* **281**, 401–419 (1964).
7. Anderson, P. W. Absence of Diffusion in Certain Random Lattices. *Phys. Rev.* **109**, 1492–1505 (1958).
8. Edwards, P. P. & Rao, C. N. R. *Metal-insulator transitions revisited.* (Taylor & Francis, London, 1995).
9. Edwards, P. P. *et al.* The metal-insulator transition: a perspective. *Phil. Trans. R. Soc. Lond. A* **356**, 5–22 (1998).
10. Edwards, P. P., Lodge, M. T. J., Hensel, F. & Redmer, R. 'a metal conducts and a non-metal doesn's'. *Phil. Trans. R. Soc. A* **368**, 941–965 (2010).
11. Redmer, R., Hensel, F. & Holst, B. *Metal-to-nonmetal Transitions.* (Springer, 2010).
12. Clérouin, J., Noiret, P., Korobenko, V. N. & Rakhel, A. D. Direct measurements and *ab initio* simulations for expanded fluid aluminum in the metal-nonmetal transition range. *Phys. Rev. B* **78**, 224203 (2008).
13. Clérouin, J. *et al.* Pressure and electrical resistivity measurements on hot expanded nickel: Comparisons with quantum molecular dynamics simulations and average atom approaches. *Phys. Rev. E* **82**, 046402 (2010).
14. Clérouin, J. *et al.* Pressure and Electrical Resistivity Measurements on Hot Expanded Metals: Comparisons with Quantum Molecular Dynamics Simulations and Average-Atom Approaches. *Contrib. Plasma Phys.* **52**, 17–22 (2012).
15. Korobenko, V. N. & Rakhel, A. D. Obsevation of a first-order metal-to-nonmetal phase transition in fluid iron. *Phys. Rev. B* **85**, 014208 (2012).
16. Korobenko, V. N. & Rakhel, A. D. Direct measurements of thermodynamic functions and electrical resistivity of fluid tungsten over a wide range of densities. *Phys. Rev. B* **88**, 134203 (2013).
17. Lindl, J. D. *et al.* The physics basis for ignition using indirect-drive targets on the National Ignition Facility. *Phys. Plasmas* **11**, 339 (2004).
18. Ragan III, C. E. Shock compressioin measurements at 1 to 7 TPa. *Phys. Rev. A* **25**, 3360–3375 (1982).
19. Nellis, W. J., Moriarty, J. A., Mitchell, A. C. & Holmes, N. C. Equation of state of beryllium at shock pressures of 0.4-1.1 TPa (4-11 Mbar). *J. Appl. Phys.* **82**, 2225–2227 (1997).
20. Cauble, R. *et al.* Absolute equation-of-state data in the 10-40 Mbar (1-4 TPa) regime. *Phys. Rev. Lett.* **80**, 1248–1251 (1998).
21. Plagemann, K. U. *et al.* Dynamic structure factor in warm dense beryllium. *New Journal of Physics* **14**, 055020 (2012).
22. Wang, C., Long, Y., Tian, M. F., He, X. T. & Zhang, P. Equations of state and transport properties of warm dense beryllium: A quantum molecular dynamics study. *Phys. Rev. E* **87**, 043105 (2013).
23. Lenosky, T. J., Bickham, S. R., Kress, J. D. & Collins, L. A. Density-functional calculation of the Hugoniot of shocked liquid deuterium. *Phys. Rev. B* **61**, 1–4 (2000).
24. Collins, L. A, V *et al.* Dynamical and optical properties of warm dense hydrogen. *Phys. Rev. B* **63**, 184110 (2001).
25. Bickham, S. R., Pfaffenzeller, O., Collins, L. A. & Kress, J. D. *Ab initio* molecular dynamics of expanded liquid sodium. *Phys. Rev. B* **58**, R11813–R11816 (1998).
26. Dejarlais, M. P., Kress, J. D. & Collins, L. A. Electrical conductivity for warm, dense aluminum plasmas and liquids. *Phys. Rev. E* **66**, 025401(R) (2002).
27. Clérouin, J., Renaudin, P., Laudernet, Y., Noiret, P. & Desjarlais, M. P. Electrical conductivity and equation-of-state study of warm dense copper: Measurements and quantum molecular dynamics calculations. *Phys. Rev. B* **71**, 064203 (2005).

28. Mazevet, S., Desjarlais, M. P., Collins, L. A., Kress, J. D. & Magee, N. H. Simulations of the optical properties of warm dense aluminum. *Phys. Rev. E* **71**, 016409 (2005).
29. Faussurier, G., Blancard, C., Renaudin, P. & Silvestrelli, P. L. Electrical conductivity of warm expanded Al. *Phys. Rev. B* **73**, 075106 (2006).
30. Kietzmann, A., Redmer, R., Hensel, F., Desjarlais, M. P. & Mattsson, T. R. Structure of expanded fluid Rb and Cs: a quantum molecular dynamics study. *J. Phys: Condens. Matter* **18**, 5597–5605 (2006).
31. Clérouin, J., Renaudin, P. & Noiret, P. Experiments and simulations on hot expanded boron. *Phys. Rev. E* **77**, 026409 (2008).
32. Calderín, L., González, L. E. & González, D. J. Static, dynamic and electronic properties of expanded fluid mercury in the metal-nonmetal transition range. An *ab initio* study. *J. Phys: Condens. Matter* **23**, 375105 (2011).
33. Smith, N. V. Classical generalization of the Drude formula for the optical conductivity. *Phys. Rev. B* **64**, 155106 (2001).
34. Nikiforov, A. F. & Novikov, V. G. *Quantum-Statistical Models of Hot Dense Matter: Methods for Computation Opacity and Equation of State.* (Springer, Berlin, 2000).
35. Kuhlbrodt, S., Holst, B. & Redmer, R. COMPTRA04-a Program Package to Calculate Composition and Transport Coefficients in Dense Plasms. *Contrib. Plasma Phys.* **45**, 73–88 (2005).
36. Mott, N. F. *Metal-Insulator Transitions. 2nd edn.* (Taylor and Francis, London, 1990).
37. Magee, N. H. *et al*. Atomic structure calculations and new Los Alamos astrophysical opacities. *Astron. Soc. Pacific Conf. Proc.* **78**, 51 (1995).
38. Kresse, G. & Hafner, J. *Ab initio* molecular dynamics for liquid metals. *Phys. Rev. B* **47**, 558–561 (1993).
39. Kresse, G. & Furthmüller, J. Efficient iterative schemes for *ab initio* total-energy calculations using a plane-wave basis set. *Phys. Rev. B* **54**, 11169–11186 (1996).
40. Bagnier, S., Blottiau, P. & Clérouin, J. Local-spin-density-approximation molecular-dynamics simulations of dense deuterium. *Phys. Rev. E* **63**, 015301(R) (2000).
41. Kresse, G. & Joubert, D. From ultrasoft pseudopotentials to the projector augmented-wave method. *Phys. Rev. B* **59**, 1758–1775 (1999).
42. Blöchl, P. E. Projector augmented-wave method. *Phys. Rev. B* **50**, 17953–17979 (1994).
43. Perdew, J. P., Ziesche, P. & Eschrig, H. *Electronic structure of solids'91*. (Akademie Verlag, Berlin, 1991).
44. Nosé, S. A unified formulation of the constant temperature molecular dynamics methods. *J. Chem. Phys.* **81**, 511 (1984).
45. Monkhorst, H. J. & Pack, J. D. Special points for Brillouin-zone integrations. *Phys. Rev. B* **13**, 5188–5192 (1976).
46. Kubo, R. Statistical-mechanical theory of irreversible processes. I. General theory and simple applications to magnetic and conduction problems. *J. Phys. Soc. Jpn.* **12**, 570–586 (1957).
47. Greenwood, D. A. The Boltzmann equation in the theory of electrical conduction in metals. *Proc. Phys. Soc. London* **715**, 585 (1958).
48. Perrot, F. New approximation for calculating free-free absorption in hot dense plasmas. *Laser Part. Beams.* **14**, 731 (1996).


## Acknowledgments

This work was supported by NSFC under Grants No. 11205019, No. 11004012, No. 11105015 and No. 11275032, by the National Fundamental Security Research Program of China, and by the Foundations for Development of Science and Technology of China Academy of Engineering Physics under Grant No. 2011A0102007 and 2012B0102012.

## Author contributions

D.L. did the calculations. D.L., P.Z., J.Y., H.L., S.Z., C.W. and Z.W. analyzed the results and wrote the paper. P.Z. and J.Y. were responsible for project planning and execution.

## Additional information

**Competing financial interests**: The authors declare no competing financial interests.

**How to cite this article:** Li, D. *et al*. Quantum molecular dynamics study of expanded beryllium: Evolution from warm dense matter to atomic fluid. *Sci. Rep.* **4**, 5898; DOI:10.1038/srep05898 (2014).